Gain properties of dye-doped polymer thin films

I. Gozhyk,[1,2] M. Boudreau,[1,6] H. Rabbani Haghighi,[3] N. Djellali,[1] S. Forget,[3] S. Chénais,[3] C. Ulysse,[4] A. Brosseau,[5] R. Pansu,[5] J.-F. Audibert,[5] S. Gauvin,[6] J. Zyss,[1] and M. Lebental[1]

[1]*Laboratoire de Photonique Quantique et Moléculaire, ENS Cachan, CentraleSupélec, CNRS, Université Paris-Saclay, 94235 Cachan, France*

[2]*Surface du Verre et Interfaces, UMR 125 CNRS/Saint-Gobain Recherche, 39 quai Lucien Lefranc, 93303 Aubervilliers, France*

[3]*Laboratoire de Physique des Lasers, Université Paris 13 and CNRS UMR 7538, 99 Avenue Jean-Baptiste Clement, F-93430 Villetaneuse, France*

[4]*Laboratoire de Photonique et Nanostructures, CNRS UPR20, Route de Nozay, F-91460 Marcoussis, France*

[5]*Laboratoire de Photophysique et Photochimie Supramoléculaires et Macromoléculaires, CNRS UMR 8531, Institut d'Alembert FR 3242, Ecole Normale Supérieure de Cachan, F-94235 Cachan, France*

[6]*Groupe de Recherche sur les Couches Minces et la Photonique, Département de Physique et d'Astronomie, Université de Moncton, Moncton, New Brunswick, Canada E1A 3E9*

Hybrid pumping appears as a promising compromise in order to reach the much coveted goal of an electrically pumped organic laser. In such configuration the organic material is optically pumped by an electrically pumped inorganic device on a chip. This engineering solution requires therefore an optimization of the organic gain medium under optical pumping. Here, we report a detailed study of the gain features of dye-doped polymer thin films. In particular we introduce the gain efficiency K, in order to facilitate comparison between different materials and experimental conditions. The gain efficiency was measured with a variety of experimental methods (pump-probe amplification, variable stripe length method, laser thresholds) in order to study several factors which modify the actual gain of a layer, namely the confinement factor, the pump polarization, the molecular anisotropy, and the re-absorption. For instance, for a 600-nm-thick 5-wt % DCM doped poly(methyl methacrylate) (PMMA) layer, the different experimental approaches give a consistent value of $K \simeq 80$-cm MW^{-1}. On the contrary, the usual model predicting the gain from the characteristics of the material leads to an overestimation by two orders of magnitude, which raises a serious problem in the design of actual devices. In this context, we demonstrate the feasibility to infer the gain efficiency from the laser threshold of well-calibrated devices. Temporal measurements at the picosecond scale were carried out to support the analysis.

I. INTRODUCTION

Photonic technology based on organic materials has continuously progressed over the last decades [1]. Organic diodes (so-called OLEDs) have developed into an industrially viable domain, whereas polymer based integrated optical devices [2–4] have matured into robust alternatives to semiconductor devices. Among their advantages are the possibility for flexible substrates [5], the quasiunlimited versatility of materials [6], and a more favorable bio- or chemical compatibility [7].

However, for more than 20 years, the direct electrical excitation of stimulated emission in organic semiconductors has remained a major challenge [8,9], although solid-state organic lasers demonstrated their high potential under optical pumping [10,11]. In fact, electrically pumped organic materials exhibit several extra loss mechanisms (triplet-induced problems [12,13], charge-induced absorption [14,15], and absorption at metal contacts), which grow rapidly with the current [8], creating a negative feedback loop [10,16].

Therefore the excitation of organic materials via an inorganic electroluminescent pump [12] is now considered as more realistic and thus as a highly promising approach, since it allows to achieve an *indirect* electrical pumping of the gain medium. Lasing in such a hybrid system was successfully demonstrated under various pumping sources: microchip lasers [19], inorganic laser diodes [20,21], and even incoherent light-emitting diodes (LEDs) [22]. Indirect electrical excitation requires to carefully examine optical pumping to take into account the specificities of these new pump sources and of organic materials. Plasmon-assisted organic emitters and especially spasers (plasmonic lasers) would also take benefit of such a study, since their gain medium often involves organic materials [23–25].

It is relatively easy to achieve lasing with laser dyes, since these small molecules are commercially available and provide stimulated emission in a great variety of host matrices. However, quantifying their lasing features is much more difficult, in particular predicting the linear gain and lasing thresholds. In this paper, we present a general perspective on the gain properties of dye-doped thin films, using several complementary approaches, such as threshold measurements, linear gain measurements, temporal measurements, and simulations. In order to provide guidelines for the comparison of organic materials, a systematic description of gain properties is introduced. In fact this field has remained largely unexplored, apart from a few works on particular concentrations of specific dye molecules [26–29]. For this purpose, our experimental test beds are dye-doped polymer thin-film lasers based on commercial laser dyes, namely DCM, Rhodamine 640 (RH640), and Pyrromethene 605 (PM605), embedded in a passive matrix, in conventional configurations such as amplified spontaneous emission (ASE) and Fabry-Perot like cavities; see Fig. 1. The method proposed herein aims at facilitating the engineering of photonic devices and providing a tool for material preselection.

The paper is organized as follows. First, Sec. II presents the samples and the optical characterization setups. Then Sec. III
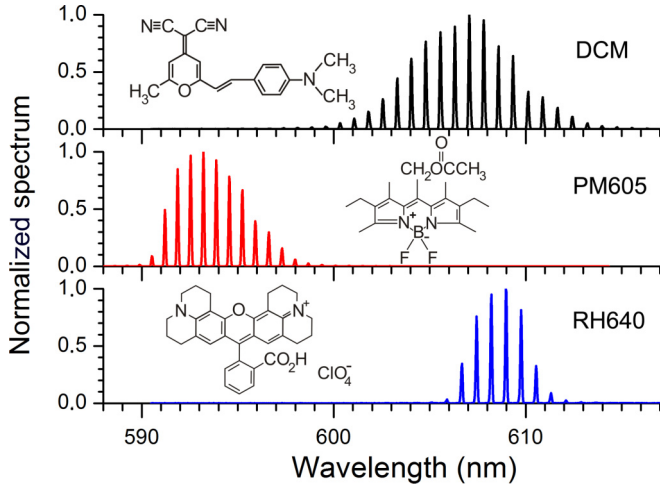
FIG. 1. (Color online) Molecular structures of the laser dyes studied in this paper, and normalized emission spectra of a 150-μm Fabry-Perot-like microlaser doped with the corresponding dye.
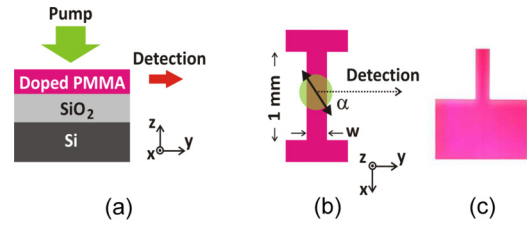

FIG. 2. (Color online) Usual sample configuration, as described in Sec. II A: (a) The sample stack, not to scale; (b) in-plane scheme of a ribbon (i.e., Fabry-Perot-like) resonator. The pumped part is indicated by a green disk. The angle between the polarization of the pump beam (double arrow) and the direction of the detection (y axis) is called α. (c) Optical microscope photo in real colors of a $w = 165\,\mu$m PMMA-PM605 ribbon microlaser (partial view, bottom part).

provides a general description of the gain, and introduces the relevant parameters, which are then studied in detail in the following sections. The specificities of the geometry are taken into account via the confinement factor and the modal gain, which are discussed and measured in Sec. IV. Based on these measured amplification properties, Sec. V provides a comparison between the experimental laser thresholds and the estimated values in the test-bed configuration of Fabry-Perot microlasers. The good agreement and the reliability of this method stress the advantage to calibrate gain measurements on laser threshold of well-controlled devices. Then, in Sec. VI the impact of the pump polarization on gain is accounted for through a model based on fluorescence anisotropy in good agreement with experiments. Spectral features influencing the evaluation of gain are finally detailed in Sec. VII. The last section, Sec. VIII, deals with the direct measurement of the bulk gain by amplification of a probe beam, which leads to an experimental value consistent with the previous ones, contrary to theoretical estimations, which overestimate the gain by two orders of magnitude.

Several appendixes provide additional descriptions of this system. Appendixes A and D deal with time-resolved experiments, while Appendixes B and C set some definitions on fluorescence anisotropy and cross sections of laser dyes.

II. EXPERIMENTAL CONFIGURATIONS

The study reported in this article is focused on actual optically pumped organic lasers made of a single polymer thin film, as presented in Fig. 2. In order to obtain a survey on their gain properties, several complementary experiments were carried out on different sample types, adapted to each experimental configuration. This section gathers information on the various experimental setups used through the paper and their typical samples. First the lasing characterization setup, the fabrication of samples, and their geometry are described. Then we detail the specificities of the samples used for amplification measurements in Sec. VIII. Finally,

both setups used for time-resolved experiments are briefly discussed, with more details given in Appendix A.

A. Laser experiments

The typical layer stack is presented in Fig. 2(a). It is made of a 600 nm thick PMMA layer [poly(methyl methacrylate), purchased from MicroChem] doped with a laser dye (5 wt %), and spin-coated on a commercial 2-μmSi0$_2$/Si wafer. For all experiments except amplification measurements (Sec. VIII), we used PMMA with a molecular weight of 495 000 at a concentration of 6 wt % in anisole. The laser dyes were bought at Exciton and used as received.

The polymer layer can be patterned by electron-beam lithography, which generates arbitrary cavity shapes with a nanoscale etching quality [30]. In Secs. V and VI, we focus on the simplest case of Fabry-Perot resonators, in order to compare threshold measurements with theoretical predictions.

The sample is pumped from the top (along the z axis; see notations in Fig. 2) by a frequency doubled Nd:YAG laser (532 nm, 500 ps, 10 Hz). Then the emitted intensity is collected at the sample edge, in the layer plane (xy plane). In fact, the index contrast between the silica and the polymer layer allows for the confinement of the electromagnetic fields within the layer plane (xy plane), while the thickness of the film is chosen to be of the order of the emission wavelength to get a single excitation along z [31].

The energy and the linear polarization of the pump beam are controlled independently with a standard combination of linear polarizers and half-wave plates. The polarization of the pump beam lies within the layer plane (xy plane) and its orientation in this plane is defined by the angle α with respect to the y axis [see Fig. 2(b)], namely $\alpha = 0°$ if the polarization is oriented along the y axis, and $\alpha = 90°$ if the pump polarization is along the x axis. The influence of α is discussed in Sec. VI. Unless otherwise specified, a pump polarization with $\alpha = 90°$ is being considered.

B. Amplification experiments

In Sec. VIII, we report the measurements of the linear material gain g_{mat} by means of a pump-probe experiment. The pump laser was identical to the above-described experiment. The

probe beam at 594 nm was sent to measure the amplification by the excited dye-doped polymer layer. Probe wavelength was chosen in the spectral region with high dye emission cross section and negligible dye absorption. The setup is further detailed in Sec. VIII.

In order to get a longer interaction path between the probe beam and the excited film, the thickness and dye concentration of the dye-doped polymer layer as well as its substrate were changed. The sample used in amplification experiment was an 18-μm PMMA layer (molecular weight 950 000, 15 wt % in anisole) doped with 1.4 wt % DCM, and spin-coated on a glass substrate.

C. Time-resolved experiments

Since organic emitters can return from the excited energy state to the ground state through different pathways [11,32,33], the experimental analysis of any emission from organic semiconductors is not complete without the characterization of the emission dynamics. For this purpose, we used two different experimental configurations.

First, a streak camera recorded the temporal behavior of usual samples (see Sec. II A), and shows the difference between fluorescence, ASE, and laser dynamics. The setup is presented in Appendix A. The main results are gathered in Fig. 15.

Then the decay of fluorescence was measured with a fluorescence-lifetime imaging microscope (FLIM), described in Appendix D. The samples were made of a 600-nm-thick PMMA layer spin-coated on a glass substrate and doped with various concentrations of laser dyes, in order to evidence the influence of quenching, as discussed in Sec. VIII.

III. GAIN IN THIN FILMS

Gain properties of active media are of utmost importance for the design of photonic devices. However, the usual gain terminology is not appropriate for comparing amplification in different organic materials under different pumping geometries. In this section, we analyze the commonly used definitions of gain and their limitations, and introduce an alternative and more relevant way to account for gain in organic thin films.

Two parameters are used in the literature to describe amplification: *material* and *modal* gain. Both describe an average growth rate of electromagnetic flux per unit medium length (in cm^{-1}, [34]), but in different systems. The *material* gain represents the gain in bulk, whereas the *modal* gain describes amplification in the exact thin-film geometry, accounting for transverse overlap of the material gain (g_{mat}) with the pump and propagating mode profiles (Γ) inside the layer [35]:

$$g_{\mathrm{mod}} = \Gamma g_{\mathrm{mat}} - \alpha_{\mathrm{mod}}. \qquad (1)$$

Modal losses α_{mod} should not be confused with material (bulk) losses α_{mat}, that will be described below. Modal losses encompass all the losses that emerge due to diffraction or scattering at the layer interfaces, i.e., losses that are not present in a homogeneous bulk medium.

In the literature, experimental gains are generally obtained in thin-film configuration with the "variable stripe length" technique (VSL) [35]. But, as a matter of fact, these are

modal gain values and are therefore strongly influenced by the sample geometry (layer thicknesses and refractive indexes), as well as experimental conditions (e.g., wavelength and orientation of the pumping beam). Thereby, despite a great number of publications on gain in organic materials, a systematic comparison of gain properties is still lacking due to variations of experimental configurations. It is possible to account for the impact of the system geometry through the estimation of the confinement factor Γ. However, this demands supplementary information, in particular the absorption and stimulated emission spectra of the material under study. An example is provided in Sec. IV B.

To reach the laser threshold, the challenge lies in getting the material gain g_{mat} greater than the losses. *A priori*, the gain of the bulk material g_{mat} is not a constant; it depends on several parameters including the wavelength and pump intensity I_p. Gain in inorganic semiconductors is known to vary logarithmically with the carriers' density, which in fact is proportional to the pump intensity, thus leading to $g_{\mathrm{mat}} \propto \ln(I_p)$ [36]. However, early works on dye lasers state that amplification in such medium is proportional to the density of excited molecules [37], which in its turn depends linearly on the density of absorbed photons. This leads to the linear dependance of the gain on pump intensity in an intensity range limited by saturation and nonlinear effects:

$$g_{\mathrm{mat}} = K I_p - \alpha_{\mathrm{mat}}, \qquad (2)$$

where α_{mat} gathers various loss mechanisms, some independent on pump intensity (traps, for instance), and some varying with the pump intensity, like polarons or excited states.

The linear coefficient K, referred to hereafter as *gain efficiency,* provides an alternate gain description. We found a confirmation of expression (2) in some publications [17,28,29,38], listing modal gain at several pump intensity values. The inferred gain efficiency K is about 10^1–10^2 cm MW^{-1} for dye-doped systems [28,29] and about 10^3 cm MW^{-1} for conjugated polymers [17]. The unit cm MW^{-1} reveals that we consider the pump intensity and not the pump fluence, following the discussion in Sec. 2.6.4 of [1].

A more comprehensive description of the material gain g_{mat} includes spectral influence, since the absorption and emission cross sections, σ_a and σ_e, depend significantly on the frequency. The consequences on gain and lasing features are described in Sec. VII. A pragmatic evaluation of both cross sections is presented in Appendix C.

In this section, we introduced the gain efficiency K to describe the amplification properties of the bulk material. It can be measured by pump-probe experiment as illustrated in Sec. VIII. However, the actual gain of a layer is modified by additional parameters: the confinement factor Γ (Sec. IV), the polarization properties (Sec. VI), and the spectral features (Sec. VII). As long as the saturation of absorption remains negligible, expression (2) is a good approximation of the material gain. In the next section, this linear dependance is experimentally confirmed in a reasonable range of pump intensities.

IV. MODAL GAIN g_{mod}

The variable stripe length (VSL) technique is commonly used as a basic method to measure the gain in a thin-film
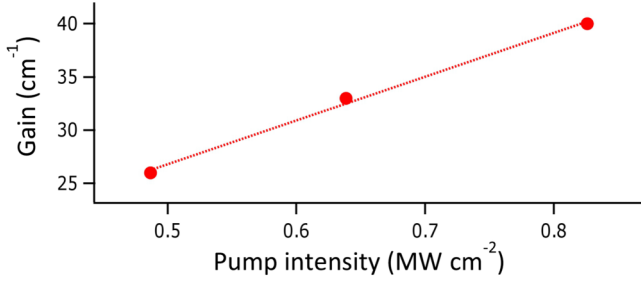
FIG. 3. (Color online) Modal gain vs pump intensity for a 600-nm-thick 5 wt % DCM doped PMMA layer on a 2-μm SiO$_2$/Si layer, measured by VSL method.

device [29,35]. In fact, it gives access to the modal gain g_{mod}, which depends on the overlap between the pumped region and the laser field. In this section, we first measure the modal gain of our usual layer stack described in Sec. II A. Then a general formulation of the confinement factor Γ is proposed and calculated for this specific case, in order to evidence the influence of the sample geometry and experimental configuration.

A. VSL method

The modal gain g_{mod} of the usual layer stack described in Sec. II A was measured by means of the variable stripe length (VSL) technique. The pump beam was shaped as a rectangle of fixed width (about 300 μm) and variable length L. Then the emitted intensity was collected at the sample edge, in the layer plane (xy plane), and the modal gain can be inferred from its variation versus the length L at a fixed pump intensity. Further details on this experiment can be found in [39]. As shown in Fig. 3 for a DCM doped PMMA layer, the modal gain varies linearly with the pump intensity, which evidences that Eq. (2) is sensible. The gain efficiency was then inferred from a linear fit: $\Gamma K = 41 \pm 2 \, \mathrm{cm} \, \mathrm{MW}^{-1}$. This value depends on the specificities of the layer stack. As shown in the next subsection, the confinement factor Γ can be numerically calculated to estimate the influence of geometrical parameters.

Even if this value of K is consistent with other experimental measurements (see below, in particular Secs. V and VIII), the VSL technique is known to be prone to artifacts [35,40].

B. Confinement factor

The confinement factor Γ was introduced in Eq. (1) in order to account for the overlap of the material gain g_{mat} with the pump E_p and lasing E_l mode profiles [41]. Therefore it depends on the specific lasing mode E_l which is considered. Equation (1) is an abridged version of an expression, which involves the integration of the spatial profiles of the fields and the gain efficiency over the volume of the gain layer. For the sake of simplicity, we assume that the field profiles are uniform within the sample plane (along x and y axes; see Fig. 2), and consider only field variations along the layer thickness (z axis), then integration occurs only along the thickness of the gain

layer h:

$$\Gamma = \frac{\int_h dz \, \tilde{f}(z) |E_l(z)|^2}{\int_\mathbb{R} dz \, |E_l(z)|^2}, \tag{3}$$

where $\tilde{f}(z)$ is the normalized function describing the distribution of the excited molecules along the z axis.

In some experiments, the gain is uniform within the layer, which means $\tilde{f}(z) = 1$ inside (for instance, no concentration variation and excitation homogeneously distributed within the layer) and null outside the layer. In this specific case, the confinement factor is defined by the ratio of the laser field overlapping the gain layer [42]:

$$\Gamma = \frac{\int_h dz \, |E_l(z)|^2}{\int_\mathbb{R} dz \, |E_l(z)|^2}. \tag{4}$$

The confinement factor varies then between 0, when there is no overlap between the laser field and the gain region, and 1, when the whole field is located within the excited layer.

However, in most configurations, the pump profile or the distribution of the material gain is not uniform within the gain layer, and this distribution must be taken into account. In this case, we consider the normalized function $\tilde{f}$ defined by

$$\tilde{f}(z) = \frac{\eta(z) |E_p(z)|^2}{\mathrm{Max}[\eta |E_p|^2]}, \tag{5}$$

where $\eta(z)$ is the density of emitters over the layer thickness (z axis) and $\max[\eta |E_p|^2]$ is the maximum value of the function $\eta(z) |E_p(z)|^2$. As $\tilde{f}$ varies between 0 and 1, the emission field acts as an envelope for $\tilde{f}(z) |E_l(z)|^2$ in Eq. (3). As a result, the upper limit of Γ becomes inferior to 1 and depends on the overlap between the emission profile and $\tilde{f}$. Moreover, Eq. (3) leads to Eq. (4) for a uniform gain, as expected.

The confinement factor can be calculated for a given geometry, for instance for the configuration of the slab waveguide presented in Fig. 2(a). For the pump field, we consider a standing-wave problem in a multilayered system: the dye-doped polymer (refractive index $n = 1.54$ and thickness $h = 600$ nm) and the SiO$_2$ layer ($n = 1.46$, $h = 2 \, \mu$m) placed between the semi-infinite medium (air, $n = 1$) and the substrate (Si, $n = 4.14$). For the propagating laser field, we use the model of the effective index described in [31], and consider the first vertical excitation with TE polarization, which means that the electric field lies in the plane of the layer. Actually, for ASE and Fabry-Perot microlasers, the laser emission is mostly TE polarized [43].

The confinement factor was numerically estimated based on Eq. (3). The pump profile $|E_p(z)|^2$ varies within the layer due to absorption. Here, we consider a fixed pump wavelength, $\lambda_p = 532$ nm, in accordance with the experiments described in this paper. Then, the confinement factor Γ depends on the wavelength because of two different physical terms, namely the profile of the laser field $|E_l(z)|^2$, and the emission cross section via $\tilde{f}$. Figure 4(b) evidences that Γ remains close to 0.5 for the specific geometry considered here. In this configuration, the variation of the confinement factors with the wavelength is quite similar for the three dyes [see Fig. 4(b)], which means that the emission wavelength in such devices will be defined by the spectral shape of the emission cross section [Fig. 4(c)].
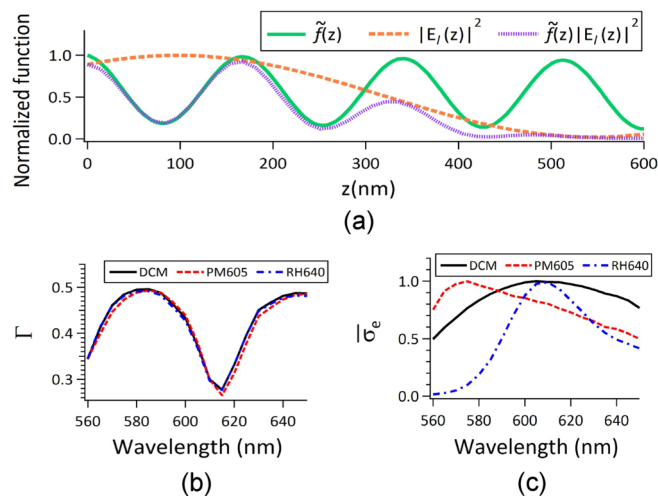
FIG. 4. (Color online) (a) Distribution of $\tilde{f}(z)$ for a 5 wt % DCM doped PMMA layer pumped at 532 nm, from Eq. (5), distribution of normalized $|E_l(z)|^2$ at 600 nm, and plot of $\tilde{f}(z)|E_l(z)|^2$. $z = 0$ stands for the air-polymer interface. The pump is only slightly absorbed by the DCM doped layer. (b) Confinement factors Γ calculated from Eq. (3) in a 600-nm-thick 5 wt % dye-doped PMMA layer for DCM, RH640, and PM605 dyes. (c) Normalized emission cross sections, inferred from Eq. (C1).

Finally, Fig. 5 presents the influence of the thickness of the dye-doped PMMA layer on the confinement factor Γ. In general, the increase of the layer thickness up to some limit value (around 900 nm) results in an increase of Γ, and thus of the gain. Actually the absorption of the pump leads to a nonhomogeneous excitation profile within the layer [see Fig. 4(a)]. Increasing the layer thickness results in the decay of the pumping field magnitude towards the substrate [Fig. 5(a)].
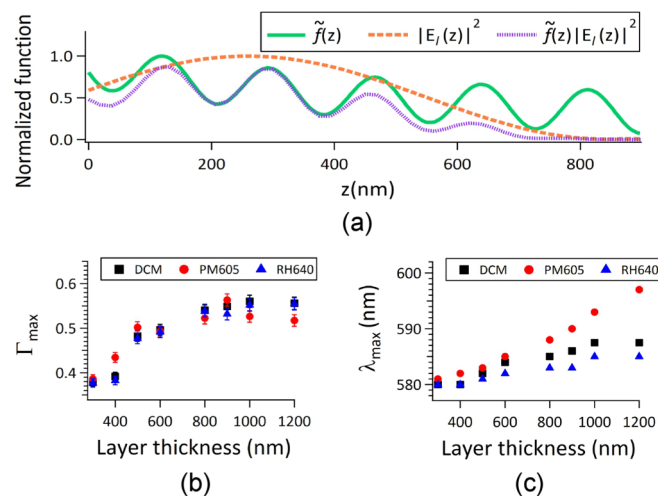

FIG. 5. (Color online) (a) Distribution of $\tilde{f}(z)$ for a 5 wt % PM605 doped PMMA layer pumped at 532 nm, from Eq. (5), distribution of normalized $|E_l(z)|^2$ at 590 nm, and plot of $\tilde{f}(z)|E_l(z)|^2$. $z = 0$ stands for the air-polymer interface. (b) Maximum of the confinement factor for the three dyes vs the thickness of the gain layer. (c) Wavelength corresponding to the maximum value of the confinement factor vs the thickness of the layer.

In the case of moderate decay of the pumping field magnitude within the layer, the overlap of the excitation and emission patterns improves. However, when the gain layer becomes strong, the excitation profile decays faster than the emission profile thus decreasing the overlap. The emission wavelength is also impacted by the layer thickness, as shown in Fig. 5(c).

C. Conclusion on modal gain

In conclusion, the amplification properties are strongly influenced by the exact geometry of the system and the confinement factor is an appropriate tool to take into account such parameters. But, to have access to the gain of the actual device, the input of the material gain g_{mat} is necessary. It can be inferred from VSL experiments, if Γ is known. For instance, in the layer stack considered here, Γ is about 0.5, which means that the gain efficiency inferred from VSL experiments was in fact $K = 82 \pm 4 \, \mathrm{cm \, MW^{-1}}$. A good agreement is evidenced in Sec. VIII. However, VSL experiments are prone to artifacts [35,40], and it is sometimes more convenient and reliable to determine the gain from laser thresholds of well-controlled devices, as shown in the next section.

V. THRESHOLD ESTIMATE

Once the gain efficiency K is known, it can be used to quantitatively predict the lasing threshold intensity of a specific device. Reciprocally, K can be inferred from threshold measurements in well-controlled configurations. This section deals with both aspects of this issue, using simple and well-known Fabry-Perot resonators.

The sample type and the characterization setup are described in Sec. II A. The gain efficiency K measured by VSL in Sec. IV A should then still be valid. To obtain a Fabry-Perot resonator, a ribbon shape was chosen. Ribbon cavities were fabricated with different widths w ranging 100–200 μm. As shown in Figs. 2(b) and 2(c), there is no border in the x direction, in order to prevent back reflection along the x axis, and therefore to avoid mode competition, which would modify the lasing thresholds. We then expect Fabry-Perot modes propagating along the y axis.

The ribbon resonator was pumped partially, as presented in Fig. 2(b). Here, we consider the most favorable case, where the polarization of the pump beam is perpendicular to the y axis, i.e., $\alpha = 90°$, like in VSL experiments described in Sec. IV A. Typical Fabry-Perot spectra are presented in Fig. 1. Their free spectral range (FSR) indicates that the lasing modes correspond indeed to Fabry-Perot resonances [31]. Figure 6(b) shows typical I-I plots, where the threshold intensity I_{th} is identified as a change of slope with a precision of about 0.1 MW cm^{-2} [44]. Then the experimental thresholds for the three dyes are gathered in Fig. 7.

To predict the threshold intensity, we assume that the stationary regime is reached. This assumption is validated *a posteriori* thanks to the good agreement with experiments. In the stationary regime, the threshold is determined by the modal gain (and thus the pump intensity) sufficient to compensate the losses:
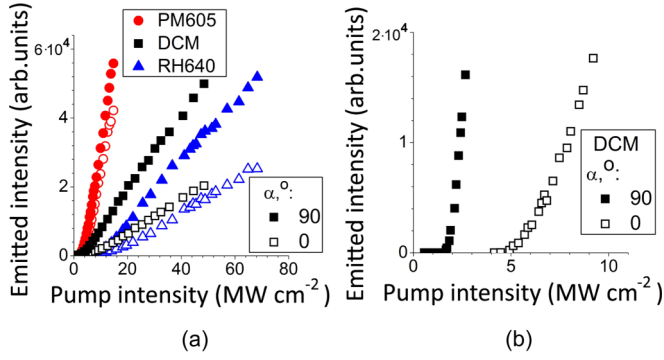
$$r e^{g_{th} 2w} = 1 \qquad (6)$$

FIG. 6. (Color online) Influence of the pump polarization α on the emission. Emission intensity vs pump intensity in the case of (a) ASE, (b) a 165-μm DCM Fabry-Perot microlaser.

TABLE I. Comparison of gain efficiencies ΓK for the three dyes inferred by fitting the experimental data of Fig. 7 with Eq. (7), using $R = 0.04$.

Dye	DCM	RH640	PM605
ΓK (cm MW^{-1})	42 ± 4	9 ± 1	81 ± 2

with r standing for the total losses in the system. For the sake of simplicity, we only consider refraction losses (the major factor of losses in our system): $r = R^2$, where $R = \left(\frac{n-1}{n+1}\right)^2 \simeq 0.04$ is the reflection coefficient at the boundary ($n_{cavity} = n \simeq 1.5$ / $n_{air} = 1$). Pump intensity at the threshold is then expected to be linear with $1/w$:

$$I_{th} = -\frac{\ln R}{\Gamma K}\frac{1}{w} + \frac{\alpha_{\rm mod}}{\Gamma K} \qquad (7)$$

using $g_{th} = g_{\rm mod} = \Gamma K I_{th}$. As reported in Fig. 7, pump intensities at threshold show indeed a linear behavior with $1/w$. Moreover, a quantitative agreement with Eq. (7) is demonstrated for DCM in Fig. 7(a), using $R = 0.04$ and $\Gamma K = 41$ cm MW^{-1}, without an adjusted parameter.

This agreement has several consequences. (i) The assumption of a stationary regime should be valid. (ii) Spatial hole burning does not influence the thresholds, whereas dye molecules lead to a homogeneous gain and the spectra are multimode, even at threshold. (iii) Only the losses due to refraction are taken into account in Eq. (7). Hence the quantitative agreement means that the losses due to diffraction at the cavity edges do not modify the thresholds, as evidenced in [45], and that the Fresnel coefficient for an infinite wall R does reproduce correctly the refraction at the boundary, even if the cavity thickness scales with the wavelength.

Figure 7 also shows a departure from a linear behavior for the smallest cavities (around 100 cm^{-1}). More intricate
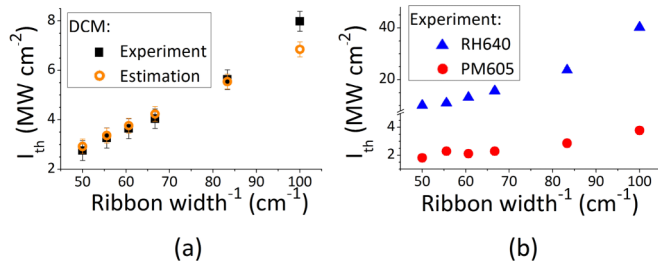

FIG. 7. (Color online) Experimental threshold intensities vs $1/w$ at $\alpha = 90°$ with different laser dyes: (a) DCM [together with estimated values from Eq. (7), using $\Gamma K = 41$ cm MW^{-1} inferred in Sec. IV A]; (b) PM605 and RH640.

active phenomena occur in these cases and will be discussed in Sec. VII.

Reciprocally, Eq. (7) can be used to infer the gain efficiency for the three dyes. The fit results are given in Table I. At first view, it would seem that PM605 is a more efficient laser dye than DCM and RH640. However, the conclusion is intricate, since the pump wavelength and the dye concentration were fixed, whereas a proper comparison would require a specific optimization for each laser dye.

To summarize, we evidenced that the gain efficiency K inferred by the VSL technique in Sec. IV A is consistent with threshold measurements of test-bed Fabry-Perot microlasers. Moreover, predictions can be made with good precision (less than 10% of uncertainty). Instead of measuring the gain by VSL or pump-probe experiments, it is hence easier and more reliable to infer K from the threshold intensity of well-controlled laser test beds, such as Fabry-Perot microlasers, the confinement factor Γ being calculated independently.

VI. INFLUENCE OF THE PUMP POLARIZATION

Absorption and emission of light in organic semiconductors are known to be strongly polarization dependent [32,33,43]. For instance, pump polarization can modify ASE intensity and laser threshold *up to a factor of 3*. It is thus essential to take this issue into account. Therefore this section focuses on the influence of the pump polarization on gain. A model is provided in quantitative agreement for the three laser dyes.

Due to the molecular structure of organic materials, amplification is in general *anisotropic* in such media [43]. In an approximate model, dye molecules in a polymer matrix can be considered as fixed and noninteracting dipoles. Each molecule absorbs preferentially along the direction of its absorption dipole, and emits a fluorescent photon according to its emission dipole. Both dipoles depend on the geometry of the molecular structure. This explains that an ensemble of dye molecules can emit fluorescence in specific directions (monitored by the pump polarization), even if they are isotropically distributed. This phenomenon is known as fluorescence anisotropy and has generated a broad literature (see [32] and [33] for reviews). This effect was used for instance in organic light emitting diodes, aligning the molecules to optimize the fluorescence emission [46,47], or in thin films to engineer the second harmonic generation and the two-photon fluorescence [48]. Here, we focus on its consequences on stimulated emission and gain. Theories were developed to account for amplification anisotropy [49–52], however we will show hereafter that it can be described in the framework of fluorescence anisotropy, in good agreement with experiments.

We experimentally investigated the influence of the pump polarization on ASE intensity and lasing thresholds with

the typical samples and the characterization setup, which are described in Sec. II A. ASE experiments were carried out on doped PMMA layers, without lithography step. As in the previous section, we consider test-bed Fabry-Perot microlasers. The direction of observation remains along the width of the ribbon (the y axis in Fig. 2(b)], while the linear pump beam polarization lies in the substrate plane and is varied between perpendicular ($\alpha = 90°$) and parallel ($\alpha = 0°$) to the y axis. Figure 6 presents the emitted intensity versus the pump intensity in ASE and Fabry-Perot configurations. It suggests that the pump polarization α is a relevant parameter, whose influence is strongly related to the molecular structure of the dye. For instance, the laser threshold is reduced by a factor of 3 from $\alpha = 0°$ to 90° for DCM [Fig. 6(b)], which can be considered as a linear dipole due to its elongated molecular structure, while the ASE curves remain almost unmodified for PM605 [Fig. 6(a)], which features a more rounded-off skeleton (see Fig. 1).

To predict the dependance on α, we use a model based on fluorescence anisotropy [33,53,54], which accounts for a given distribution f of fixed and noninteracting dyes. The emitted intensity I_e is proportional to an integral over all the possible orientations Ω of a molecule:

$$I_e(\alpha) \propto \int_\Omega P_{\mathrm{abs}}(\alpha, \Omega) P_{em,y}(\Omega) f(\Omega) d\Omega. \tag{8}$$

Here P_{abs} stands for the probability of pump absorption and is then proportional to a cosine squared between the pump polarization and the absorption transition dipole of the molecule. Likewise $P_{em,y}$ stands for the emission probability in the y direction and is then a sinus squared between the y direction and the transition emission dipole of the molecule. Hence we must introduce the angle β between the absorption and emission transition dipoles of the molecule, which is known to be a constant, depending only on the molecular structure of the dye [55].

To calculate expression (8), we must choose an appropriate distribution f. For instance, f is constant for an isotropic distribution of molecules. As evidenced by ellipsometry measurements, spin coating slightly aligns the molecules in the layer plane. So we introduce an angle θ_0, such that f is constant between $-\theta_0$ and $+\theta_0$ and zero outside (see Fig. 16). A more comprehensive study is reported elsewhere [53]. Here we skip the details and go directly to the following formula [56]:

$$\frac{I_e(\alpha)}{I_e(\alpha = 90°)} = \frac{\rho + 1}{2} + \frac{\rho - 1}{2} \cos 2\alpha, \tag{9}$$

where

$$\rho = \frac{I_e(0°)}{I_e(90°)} \tag{10}$$

is a positive function of θ_0 and $\cos^2 \beta$, and is described in Appendix B. As expected, the emitted intensity I_e is maximal for $\alpha = 90°$, which was the configuration considered for VSL and threshold measurements (Secs. IV A and V). For a linear dipole ($\beta = 0$) and an isotropic three-dimensional (3D) distribution ($\theta_0 = 90°$), then $\rho = 1/2$, which means that a significant part of the light is emitted in the y direction, even if the pump polarization is parallel to the y direction.
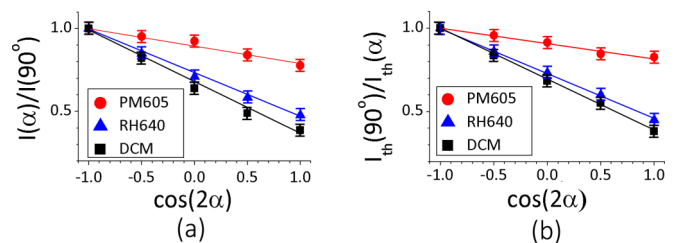

FIG. 8. (Color online) Role of the pump polarization on stimulated emission. (a) ASE in dye-doped PMMA thin film. (b) 180-μm Fabry-Perot microlasers. The pump beam polarization α is defined on Fig. 2(b).

$I_e(\alpha)$ describes the probability of fluorescence emission. Hence it is likely that the ASE intensity is proportional to I_e. First we checked that the ratio $\frac{I_e(\alpha)}{I_e(90°)}$ does not significantly depend on the pump intensity, namely the fluctuations remain in the range of $\pm 1\%$ for pump intensity varying from 4 to 80 MWcm^{-2}. The average ratio $\frac{I_e(\alpha)}{I_e(90°)}$ is then plotted versus $\cos(2\alpha)$ in Fig. 8(a) for the three dyes in the ASE regime. The curves present a linear behavior, evidencing the validity of formula (9), even in the stimulated emission regime. The ρ values presented in Table II are then inferred from the linear fits and formula (9).

Validity of Eq. (9) can be checked for lasing thresholds as well. In fact they can be considered as working points where the nonlinear behavior is still relatively low and a fluorescence formula like Eq. (8) should then apply [54,57]. The gain value g_{th} necessary to reach the lasing threshold in the stationary regime is determined by losses, which do not depend on α, leading to $\Gamma K(\alpha) I_{th}(\alpha) = g_{th} = $ const. Thereby, we expect the ratio of threshold intensities $I_{th}(\alpha)/I_{th}(90°)$ of the ribbon-shaped microlasers to be inversely proportional to $K(\alpha)/K(90°)$. Besides, the emission intensity $I_e(\alpha)$ should be proportional to $K(\alpha)$, at least in the linear regime close to threshold. Therefore $K(\alpha)/K(90°)$ should be proportional to the right part of Eq. (9), as well as $I_{th}(90°)/I_{th}(\alpha)$. This latter ratio is plotted versus $\cos(2\alpha)$ in Fig. 8(b) for $w = 180\,\mu$m Fabry-Perot microlasers and shows indeed a linear behavior for the three dyes. So a ρ value can be inferred for each of the dyes from the right part of Eq. (9). The results are gathered in Table II where the error bars correspond to the fluctuations for ribbon widths varying from 150 to 200 μm.

Experimental results, presented in this section, were obtained under linear pump beam polarization. In fact, emission under circularly polarized excitation can be described in the same terms based on Eq. (9). In fact, integration over α provides $\frac{I(\mathrm{circular})}{I(\alpha = 90°)} = \frac{\rho + 1}{2} < 1$, implying that a circularly polarized pump is less efficient than a linearly polarized one with $\alpha = 90°$. This ratio was verified for a 165-μm DCM

TABLE II. Comparison of ρ values obtained from ASE and laser threshold.

ρ	DCM	PM605	RH640
ASE	0.33 ± 0.03	0.77 ± 0.03	0.46 ± 0.03
Threshold	0.38 ± 0.03	0.84 ± 0.03	0.48 ± 0.04

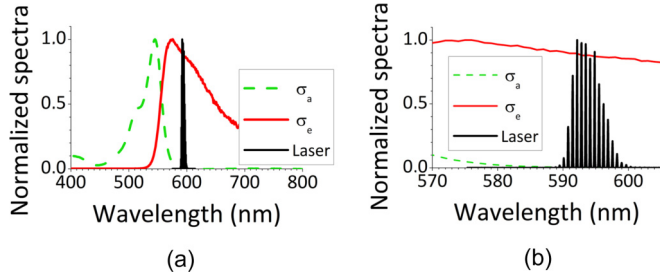(a)   (b)

FIG. 9. (Color online) Absorption and emission properties for PM605. (a) Normalized absorption cross section σ_a, normalized stimulated emission cross section σ_e, and normalized laser spectrum of a 150-μm Fabry-Perot microlaser. (b) Zoom of (a).

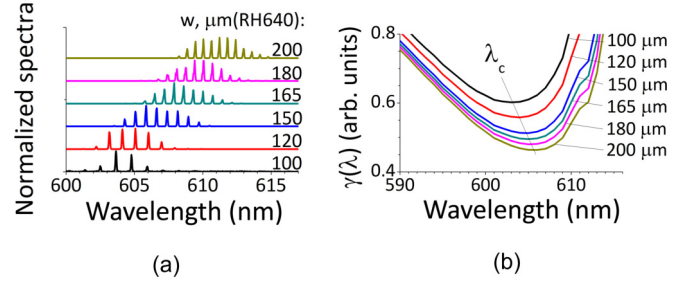(a)   (b)

FIG. 10. (Color online) Influence of losses on the spectral envelope: (a) Experimental spectra of Fabry-Perot cavities of different widths w under the same pump intensity. The experiments were carried out with a usual sample made of RH640 and the usual setup, as described in Sec. II A. (b) Threshold condition $\gamma(\lambda)$ calculated with Eq. (12) for Fabry-Perot cavities of different widths.

ribbon microlaser and gave a ρ value identical to that in Table II.

For the sake of completeness, ρ values should be inferred as well in the fluorescence regime. However the high doping rate of the layers favors energy transfer from an excited dye molecule to a neighbor dye molecule and tends to make the emission isotropic [58]. Such a tendency towards isotropy ($\rho = 1$) does not occur obviously in our stimulated systems (ASE and laser). Actually energy transfer is prevented, since its characteristic time, typical of spontaneous processes, is much longer than stimulated emission. The different time scales are evidenced in Appendix A.

To summarize, the ρ parameter quantifies the sensitivity to polarization. It is specific to a dye molecule and its distribution in the layer. Such agreement between the ρ values inferred from both ASE and lasing experiments for the three dyes stresses the validity of our assumptions as well as the interest of such an approach for predictions of gain properties. In practice, the pump polarization must be carefully controlled to optimize the gain of an organic layer, up to a factor of 3.

VII. SPECTRAL FEATURES

Laser spectra from organic-based devices are in general multimode and inscribed in an envelope (see Fig. 1). The distribution of the lasing frequencies is mostly determined by the resonator shape and is discussed elsewhere [59]. Here, we focus on the envelope, in particular its central wavelength, which depends on the gain medium and is relevant for designing an actual device.

Figure 9 evidences that the envelope of the lasing spectrum is not centered at the maximum of the fluorescence spectrum. Here, following Mazumder *et al.* [60], we propose a simple explanation based on reabsorption. Due to the overlap between absorption $\sigma_a(\lambda)$ and stimulated emission $\sigma_e(\lambda)$ cross sections, unexcited molecules can absorb photons emitted from excited states, which decreases the gain:

$$g(\lambda) = \sigma_e(\lambda)N^* - \sigma_a(\lambda)(N - N^*), \qquad (11)$$

where N stands for the total density of dye molecules and N^* for the density of excited dye molecules. Hence, the ratio of molecules $\gamma(\lambda) = N_{th}^*/N$ that must be excited to reach the

threshold depends on reabsorption [37,60]:

$$\gamma(\lambda) = \frac{N_{th}^*}{N} = \frac{g_{th}(\lambda) + \sigma_a N}{\sigma_e N + \sigma_a N}. \qquad (12)$$

At threshold, in the stationary regime, the gain balances the losses, and $g_{th}(\lambda)$ can be substituted by $-\ln R/\Gamma w$ for a Fabry-Perot resonator [see Eq. (6)]. $\gamma(\lambda)$ was plotted in Fig. 10(b) for different widths w of the Fabry-Perot ($\ln R$ and Γ remain unchanged) using σ_e and σ_a determined in Appendix C. Each curve shows a minimum, which corresponds to the lasing wavelength close to threshold. The minimum of γ is blueshifted when the width of the Fabry-Perot decreases, i.e., when the loss of the cavity increases. The order of magnitude is consistent with the experimental observations summarized in Fig. 10(a). A similar effect was reported using absorbers in microdroplets [60,61].

In other words, the envelope of the lasing spectrum is blueshifted when the quality factor of the resonator decreases [26]. Measurements of such spectral shifts for a given gain material would provide a solid basis for the experimental estimation of the cavity properties through the spectroscopic study of the laser effect. Anyway, as such shift can exceed a dozen nanometers, it must be taken into account to optimize the architecture of an actual device.

VIII. MEASUREMENT OF THE MATERIAL GAIN g_{mat}

The ultimate and most direct way to know the material gain g_{mat} is to measure the amplification of the layer in a simplified geometry. Therefore in this section, we report the measurement of the material gain g_{mat} by the means of a pump-probe experiment, and then its estimation based on intrinsic characteristics of the gain medium.

A. Pump-probe experiment

We carried out pump-probe experiments to get the amplification factor, and then g_{mat}. The setup is summarized in Fig. 11. In this configuration, the pump and the probe beams propagate roughly perpendicular to the sample plane. As described in Sec. II B, the sample was similar to the usual ones, but optimized for amplification: (i) the gain layer was 18 μm thick to increase the amplification path, and (ii) the concentration
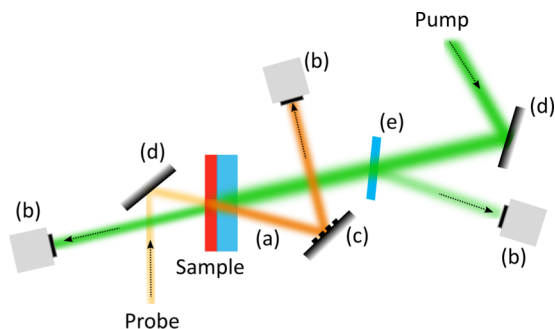
FIG. 11. (Color online) Pump-probe setup for measuring the material gain g_{mat}. Continuous probe beam and pulsed pump beam. (a) Amplified probe beam. (b) Photodiodes. (c) Monochromator. (d) Mirrors. (e) Glass slide.

of DCM was set to 1.4 wt % to distribute the absorption of the pump over the whole thickness. The pump beam was the same as for microlasers tests (532 nm, 10 Hz, 0.5 ns) with a diameter of 200 μm full width at half maximum on the sample, measured with an imaging system. The probe beam is from a helium/neon laser (594 nm, continuous, $\varnothing$ 65 μm). Both beams are incident on the sample at the Brewster angle to avoid parasitic reflections. They are not exactly parallel for experimental convenience, but their linear polarizations are parallel. The probe is collected on a rapid photodiode (rise time about 1 ns), its signal being sent to a 1-GHz oscilloscope triggered by the pump. A bump is visible when the pump is on. A typical trace is presented in Fig. 12(a). Several tests were performed to ensure that the bump rightly comes from the probe amplification. In particular, a monochromator showed that there is no bump out of the probe wavelength (i.e., 594 nm). Therefore the bump does not originate from fluorescence, but from stimulated emission.

To infer the material gain g_{mat} and the gain efficiency K from the amplification factor $\Delta A/A$ measured experimentally (Fig. 12), we use the equation of propagation for the probe intensity I_{pr}:

$$dI_{pr} = g_{\mathrm{mat}} I_{pr}\, dz = K I_p I_{pr}\, dz, \tag{13}$$

which depends on the pump intensity I_p. Assuming that the absorption of the probe is not saturated and remains linear within the thickness h of the layer—a more realistic situation
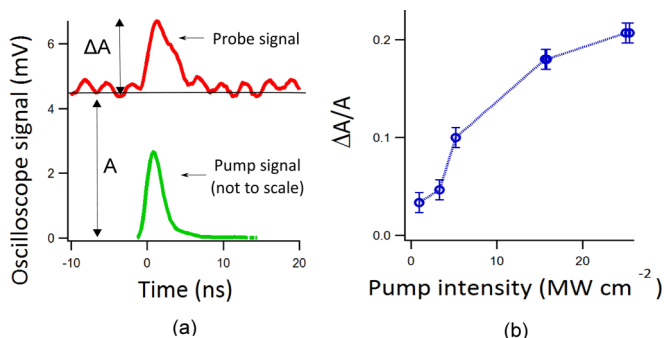

FIG. 12. (Color online) (a) Typical signals of the probe and pump beams detected by the photodiodes. (b) Amplification factor vs the pump intensity for a probe intensity $I_{pr} = 435$ W cm^{-2}.
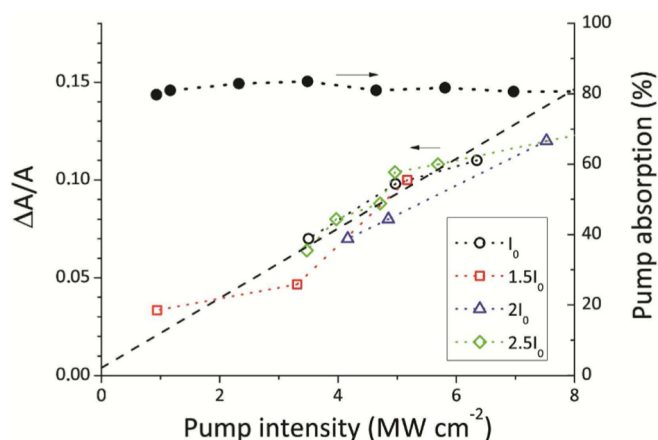

FIG. 13. (Color online) Amplification factor $\Delta A/A$ (left axis) and absorption (right axis) vs pump intensity. The dotted line is a linear fit of the set of amplification factors measured at different probe intensities, with $I_0 = 291$ W cm^{-2}.

is treated hereafter—then

$$\frac{I_{pr}(h)}{I_{pr}(0)} = \frac{A + \Delta A}{A} = e^{K I_p h}. \tag{14}$$

As the amplification factor $\Delta A/A$ is smaller than 1 [see Fig. 12(a)], then, in a linear approximation, it is proportional to the gain efficiency K:

$$\frac{\Delta A}{A} = K I_p h. \tag{15}$$

In practice, the absorption of the pump beam must be taken into account. Similar considerations lead to the conclusion that the thickness h of Eq. (15) must be replaced by an effective one:

$$h \rightarrow h_{\mathrm{eff}} = \frac{1 - e^{-\alpha h}}{\alpha},$$

where α is the absorption coefficient of the material at the pump wavelength: $\alpha = N\sigma_a(\lambda = 532\text{ nm})$. With the parameters of this experiment, the correction corresponds to the absorption of the pump over an effective thickness $h_{eff} = 9\ \mu$m, i.e., half the actual layer thickness.

As the temporal behavior of the amplification reproduces the temporal profile of the pump [see Fig. 12(a)], the variation ΔA was measured at the maximum of the bump signal, and the factor I_p involved in Eq. (15) is the peak intensity of the pump at the entrance of the layer. The measured amplification factor $\Delta A/A$ versus the peak intensity I_p is plotted in Fig. 13 for different probe intensities. The whole set of experimental data is linearly fitted, the slope being proportional to the gain efficiency K, leading to $K = 20 \pm 5$ cm MW^{-1}. Here the main source of uncertainty comes from the temporal profile of the pump beam (assumed to be Gaussian) and its duration.

In summary, amplification measurements with a 1.4-wt % DCM doped layer give $K \simeq 20$ cm MW^{-1}, while measurements by VSL technique (Sec. IV A) and laser thresholds (Sec. V) with a 5-wt % DCM doped layer lead to $K \simeq 80$ cm MW^{-1}. A linear extrapolation from 1.4 wt % to 5 wt %

gives a slightly different value, $K \simeq 70\,\mathrm{cm\,MW^{-1}}$, which is consistent with the precision of the measurements.

B. Estimation of the gain efficiency

In addition, the gain efficiency K can be predicted from the material characteristics, which is *a priori* more convenient than carrying out experiments. However, we show in this section that predictions significantly overestimate the gain.

The material gain at the wavelength 594 nm is given by

$$g_{\mathrm{mat}}^{594} = \sigma_e^{594} N^*,$$

where N^* is still the density of excited molecules. The vibrational states are known to relax in less than 1 ps [32,33], therefore much faster than the time scale involved in this study. We assume then that the dye molecules can be considered as an effective two-level system, where N_0 is the density of dye molecules in the ground state and $N = N_0 + N^*$ is the density of all the dye molecules. The triplet states are neglected, since the time scale involved in this study (see Appendix A) is much shorter than the typical time for intersystem crossing. The rate equation for N^* follows then

$$\frac{dN^*}{dt} = \sigma_a^{532} N_0 \frac{I_p}{h\nu_p} + \sigma_a^{594} N_0 \frac{I_{pr}}{h\nu_{pr}} - \sigma_e^{594} N^* \frac{I_{pr}}{h\nu_{pr}} - \frac{N^*}{\tau_f}, \tag{16}$$

where τ_f is the lifetime of fluorescence. Laser threshold experiments reported in Sec. V are consistent with the assumption of a stationary regime. Hence we still consider this assumption here, and the left part of Eq. (16) is canceled out. Then N^* can be expressed as

$$N^* = N \frac{\sigma_a^{532} \frac{I_p}{h\nu_p} + \sigma_a^{594} \frac{I_{pr}}{h\nu_{pr}}}{\sigma_a^{532} \frac{I_p}{h\nu_p} + \sigma_e^{594} \frac{I_{pr}}{h\nu_{pr}} + \frac{1}{\tau_f}}. \tag{17}$$

The cross sections are evaluated in Appendix C. The second term in the numerator of N^* is several orders of magnitude smaller than the first one, and is thus neglected. Similarly, as $I_{pr}/I_p \sim 10^{-4}$, the second term in the denominator is neglected, leading to

$$N^* = N \frac{\sigma_a^{532} \frac{I_p}{h\nu_p}}{\sigma_a^{532} \frac{I_p}{h\nu_p} + \frac{1}{\tau_f}}. \tag{18}$$

The linear regime presented in Fig. 13 corresponds to the case

$$\sigma_a^{532} \frac{I_p}{h\nu_p} \ll \frac{1}{\tau_f} \tag{19}$$

which means that I_p should be less than 8 MW cm^{-2}, in agreement with Fig. 12(b). In the linear regime, expression (18) leads to the following expression for the gain efficiency:

$$K = \sigma_e^{594} \frac{N^*}{I_p} = \sigma_e^{594} \sigma_a^{532} N \frac{\tau_f}{h\nu_p}. \tag{20}$$

In Appendix D, τ_f was measured and is about 2 ns. The other quantities involved in expression (20) are estimated in Appendix C, and lead to $K \simeq 2000\,\mathrm{cm\,MW^{-1}}$, so 100 times higher than the experimental value.

This estimation leads to two major conclusions. (i) The derivation of expression (20) was not specific to the DCM dye.

Moreover, the numerical values used to estimate K correspond to the properties of DCM, but do not change significantly from one dye to another. Hence, the estimation of the gain efficiency $K \sim 2000\,\mathrm{cm\,MW^{-1}}$ is roughly independent of the laser dye, under the assumption of a stationary and linear regime. (ii) This strong discrepancy between the estimated and measured gain efficiencies may be explained by different factors. In fact, several loss processes were not taken into account in the derivation of expression (20), like for instance absorption by excited states, reabsorption, and quenching, whereas they were evidenced in Sec. VII and Appendix D.

Furthermore, numerical simulations based on the Tang-Statz-deMars rate equations [62,63] lead to a gain which depends significantly on the pump duration and the involved losses. In general, the assumption of stationary pumping overestimates the gain efficiency. However the actual dynamics and loss processes are difficult to quantify and strongly depend on the specific thin film which is investigated. For instance, the presence of aggregates—which leads to quenching—is strongly dependent on the fabrication process [64].

We conclude this section by pointing out that the material gain g_{mat} can be effectively measured by the means of a pump-probe setup, leading to a gain efficiency of $K = 20\,\mathrm{cm\,MW^{-1}}$ at 594 nm for 1.4 wt % of DCM in PMMA pumped at 532 nm. This result is in good agreement with the experimental values inferred from the VSL method in Sec. IV A and laser thresholds in Sec. V. The predicted K is two orders of magnitude higher. However this estimation must be treated with care, since it does not include the dynamics and intra- and intermolecular processes which reduce the gain significantly and cannot be easily quantified.

IX. CONCLUSION

In this paper, we have investigated the amplification properties of dye-doped polymer thin films. The gain efficiency K was introduced to facilitate the comparison between different materials in various configurations. It represents the linear ratio between gain and pump intensity, in the limit of validity of such a linear behavior. It was consistently measured by different methods (pump-probe amplification experiment, VSL technique, laser thresholds), and is about 80 cm MW^{-1} around 600 nm for a 5% DCM-doped PMMA layer pumped at 532 nm with 0.5-ns pump pulses. A rough theoretical prediction overestimates its value by two orders of magnitude. Refinements of this model lead to gain values in better agreement, but they depend on different features of the dye-doped thin film which can hardly be measured quantitatively.

Several parameters alter the bulk gain and must be taken into account to design an actual device. First, the confinement factor Γ includes the geometrical features and the overlap between the pump beam and the propagating laser field. It varies typically from 0.3 to 0.8. Then, the intrinsic anisotropy of the molecular structure induces a sensitivity to the polarization of the pump beam, and can modify the gain up to a factor of 3. Incidentally, we showed that the gain measurement is sensitive to the anisotropic distribution of the dye molecules within the layer, and provides therefore an indirect method of estimation. Finally, the gain spectrum is monitored by
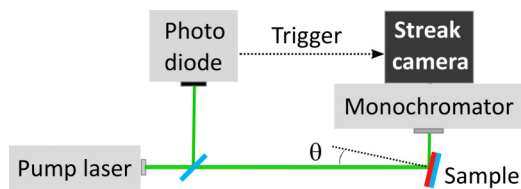
FIG. 14. (Color online) Scheme of the setup used for temporal studies. The retardation line is not shown. For ASE and Fabry-Perot measurements, θ is set to zero, and the emission is collected in the plane of the layer. For fluorescence measurements, $\theta = 55°$ in order to prevent propagation effects.

reabsorption processes and its central wavelength can be predicted relatively well. For all these parameters, we performed relevant experiments which are mutually consistent and also in agreement with theoretical predictions.

In conclusion, we showed that a theoretical prediction of gain is in general not reliable. In fact, the actual gain depends strongly on quenching and on the anisotropy of the dye distribution, which are monitored by the fabrication process of the layer. Therefore, we propose to evaluate the gain properties by comparison with well-known calibrated devices, such as the Fabry-Perot microlasers reported here. We hope that this work will help to pave the way towards an electrically pumped hybrid organic-inorganic laser.

APPENDIX A: TEMPORAL BEHAVIOR

This appendix focuses on experimental studies of the temporal properties of spontaneous and stimulated emission in dye-doped polymer thin films. The usual dye-doped PMMA layers described in Sec. II A were pumped with a frequency doubled Nd:YAG laser (10 Hz, 532 nm, 35 ps) and the emission was collected through a monochromator and then injected into a streak camera (Optoscope by ARP) with about 8 ps temporal resolution. Figure 14 presents a simplified scheme of the setup. In order to prevent the influence of guiding effects, the layers used for fluorescence study were directly spin coated on a Si substrate and θ was set to 55°, while a SiO$_2$/Si substrate was used for ASE and Fabry-Perot samples with $\theta = 0°$.

As evidenced in Fig. 15, the temporal behavior of the ASE signal replicates that of the pump (except for RH640, which exhibits a small exponential relaxation of ASE, not shown here), whereas the fluorescence emission occurs over a longer time scale. Regarding the lasing emission from a Fabry-Perot cavity, Fig. 15(b) evidences that it is delayed by some 20 ps. This delay decreases if the pump intensity increases and the Fabry-Perot width w decreases, as expected since the buildup time of the laser emission decreases as well. It can be noticed that no spiking is observed at a 100-ps scale, contrary to [27], maybe due to the shorter pump pulse.
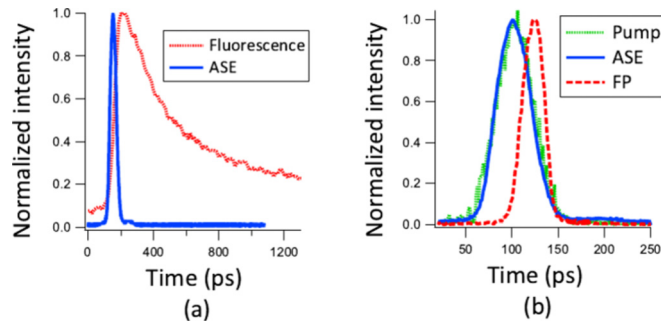

FIG. 15. (Color online) Dynamics of the spontaneous and stimulated emissions in a PMMA layer doped with 5 wt % of DCM: (a) fluorescence and ASE, (b) pump signal, ASE, and lasing emission from a Fabry-Perot cavity of width $w = 200$ μm just above the threshold. Averaging over 20–100 pump pulses.

APPENDIX B: FLUORESCENCE ANISOTROPY

This appendix provides the expression of the ρ factor mentioned in Sec. VI. We consider an ensemble of fixed and noninteracting fluorophores, and are looking for the emitted intensity in the y direction, I_e, depending on the polarization of the linear pump beam α [see Fig. 2(b) for notations]. ρ is defined as $I_e(\alpha = 0)$ normalized by $I_e(\alpha = \pi/2)$,

$$\rho = \frac{I_e(\alpha = 0)}{I_e(\alpha = 90)},$$

and was introduced to simplify formula (9).

In practice, ρ depends on two parameters, namely the distribution of dyes and the angle β between the absorption and emission dipole moments, which is roughly constant for a given dye. Here we chose an isotropic distribution of dyes within an angle θ_0, as depicted in Fig. 16. Then, the limit case $\theta_0 = \pi/2$ corresponds to a three-dimensional isotropic distribution, and $\theta_0 = 0$ to a bidimensional distribution, where the dyes lie within the layer plane, which most likely applies to spin-coated light-emitting polymers [65].

A comprehensive derivation is described elsewhere [53], the final formula being as follows:

$$\rho = \frac{A_1(\beta)B_1(\theta_0) + A_2(\beta)B_2(\theta_0)}{A_1(\beta)B_1(\theta_0) + A_2(\beta)B_3(\theta_0)}, \quad \text{(B1)}$$

where the functions $A_i(\beta)$ and $B_i(\theta_0)$ are defined by

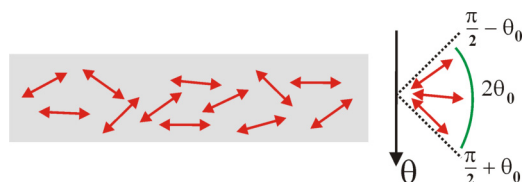$$A_1(\beta) = 2 - 2\cos^2\beta,$$

$$A_2(\beta) = 1 - 3\cos^2\beta,$$

FIG. 16. (Color online) Definition of θ_0. Left: Scheme of a polymer layer with randomly distributed fluorophores (not to scale). Right: θ_0 is defined such as each dye is orientated between $-\theta_0$ and $+\theta_0$.

$$B_1(\theta_0) = 30 + 10 \sin^2 \theta_0,$$

$$B_2(\theta_0) = -15 - 10 \sin^2 \theta_0 + 9 \sin^4 \theta_0,$$

$$B_3(\theta_0) = -45 + 10 \sin^2 \theta_0 + 3 \sin^4 \theta_0,$$

and are introduced for the sake of compacting Eq. (B1). In limit cases of 2D ($\theta_0 = 0$) and 3D ($\theta_0 = \pi/2$) distributions, the expression of ρ reduces to

$$\rho_{2D}(\beta) = \frac{3 - \cos^2 \beta}{1 + 5 \cos^2 \beta},$$

$$\rho_{3D}(\beta) = 2 \frac{2 - \cos^2 \beta}{3 + \cos^2 \beta}.$$

For instance, in the case of a 2D distribution and parallel dipole moments for absorption and emission (i.e., $\beta = 0$), then $\rho = 1/3$. For DCM, it was reported in [58] that $\beta = 25°$ under excitation at 461 nm. Assuming a 2D distribution of chromophores leads to $\rho = 0.43$.

APPENDIX C: ABSORPTION AND STIMULATED EMISSION CROSS SECTIONS

In this appendix, the values of the absorption and emission cross sections are inferred from experimental data.

1. Absorption cross section

The factor $\sigma_a(532)N$ is inferred from the absorption of the pump; see Fig. 13:

$$e^{-\sigma_a(532)Nh} \simeq 0.2 \rightarrow \sigma_a(532)N \simeq 9 \times 10^2 \text{ cm}^{-1},$$

where $h = 18 \text{ }\mu\text{m}$ is the thickness of the layer in the configuration of Fig. 13.

2. Emission cross section

The emission cross section is shaped as the fluorescence spectrum $E(\lambda)$ and given by the following formula [1,37]:

$$\sigma_e(\lambda) = \frac{\phi \lambda^4}{8\pi n^2 c \tau_{rad}} \frac{E(\lambda)}{\int E(\lambda) d\lambda}, \qquad \text{(C1)}$$

where c is the velocity of light in the vacuum. If we assume that fluorescence is the only decay channel from the S_1 excited state, then the quantum yield ϕ is equal to 1, and the radiative lifetime τ_{rad} is equal to the fluorescent lifetime measured in Appendix D, $\tau_{rad} \simeq 2$ ns. Formula (C1) is based on two main assumptions, which seems valid in this study: (i) the emission occurs from the lowest vibrational state of the S_1 band, and (ii) the density of electromagnetic modes is purely classical, without quantum confinement effect. With a refractive index $n = 1.5$, formula (C1) leads to

$$\sigma_e(\lambda = 594 \text{ nm}) \simeq 4 \times 10^{-16} \text{ cm}^2.$$

It must be emphasized that the value of σ_e cannot change very much from one molecule to another one, since the refractive index is typically 1.5–2, the radiative lifetime is about 1 ns, and the fluorescence spectrum is about 50 nm wide. Hence,
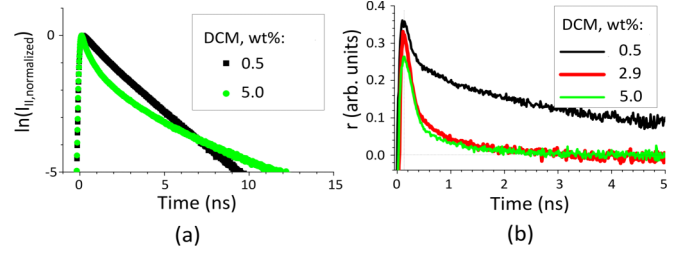

FIG. 17. (Color online) Dynamics of fluorescence for several concentrations of DCM in a PMMA layer: (a) $I_\parallel$ component of the fluorescence intensity. It is polarized along the polarization of the pump, in contrast to $I_\perp$, which is polarized orthogonally to the pump. (b) Polarization anisotropy parameter $r = (I_\parallel - I_\perp)/(I_\parallel + 2I_\perp)$ a standard fluorescence anisotropy parameter.

formula (C1) leads to more or less the same emission cross section whatever is the dye.

APPENDIX D: EVIDENCES OF AGGREGATES AND FLUORESCENCE LIFETIMES

In this appendix, we report experiments evidencing the presence of aggregates in the dye-doped layer. Actually these aggregates quench the emission, and then lead to a decrease of the gain.

Experiments were carried out with different doping rates of DCM in a PMMA layer spin-coated on a glass slide. The excitation was provided by a frequency doubled Yb:KGW laser (10 MHz, 400 fs) and the fluorescence was collected by a time-resolved single-photon counting photomultiplier (QA, Europhoton Gmbh). The setup is described in [66] and was initially dedicated to the study of the relaxation of fluorescence anisotropy. Here, we consider only data related to evidences of aggregates.

Figure 17 presents the dynamics of fluorescence for two dye concentrations. For 0.5 wt % of DCM, the plot is linear in logarithmic scale, which corresponds to a monoexponential decay, as expected for single dye molecules. For 5 wt % of DCM, the plot is obviously not linear, which evidences the presence of dye aggregates in the layer. Moreover the shape of the curve is in good agreement with the usual theory [67]. Actually, depending on the geometrical arrangement of the dye molecules inside an aggregate, the fluorescence rate is either increased (J aggregates) or slowed down (H aggregates). Indeed, the slope of the curve with 5 wt % of DCM is first higher and then lower than the slope of the curve with 0.5 wt % of DCM, which evidences the presence of both types of aggregates.

This observation is fully consistent with a systematic study of dye aggregation reported in [64]. In fact, to optimize the optical quality of the dye-doped PMMA layer, it is annealed at 120 °C, i.e., above the T_g of PMMA. As reported in [64], this process "leads to irreversible phase separation and the formation of dye aggregates."

In consequence, the fluorescence lifetimes were measured with slightly doped layers (0.5 wt %), and lead to 1.8 ns for DCM, 2.6 ns for RH640, and 1.5 ns for PM605, consistent with measurements reported elsewhere [68].

[1] S. Chénais and S. Forget, *Organic Solid-State Lasers* (Springer, Berlin, Heidelberg, 2013).

[2] S. Miyata and H. Sasabe, *Poled Polymers and Their Application to SHG and EO Devices*, 1st ed. (Australia: Gordon and Breach, 1997).

[3] S. Miyata and H. S. Nalwa, *Organic Electroluminescent Materials and Devices*, 1st ed. (CRC, Boca Raton, 1997).

[4] J. Shinar, *Organic Light-Emitting Devices: A Survey* (Springer, New York, 2004).

[5] Y. Koike, Microoptics and photonics polymer, Jpn. J. Appl. Phys. **47**, 6629 (2008).

[6] J. Mater. Chem., Organic nonlinear optics, special issue **19**, 7381 (2009).

[7] C. Y. Chao, W. Fung, and L. J. Guo, Polymer microring resonators for biochemical sensing applications, IEEE J. Sel. Top. Quantum Electron. **12**, 134 (2006).

[8] I. D. W. Samuel, E. B. Namdas, and G. A. Turnbull, How to recognize lasing, Nat. Photon. **3**, 546 (2009).

[9] M. Segal, M. A. Baldo, R. J. Holmes, S. R. Forrest, and Z. G. Soos, Excitonic singlet-triplet ratios in molecular and polymeric organic materials, Phys. Rev. B **68**, 075211 (2003).

[10] I. D. W. Samuel and G. A. Turnbull, Organic semiconductor lasers, Chem. Rev. **107**, 1272 (2007).

[11] S. Chenais and S. Forget, Recent advances in solid-state organic lasers, Polym. Int. **61**, 390 (2012).

[12] M. A. Baldo, R. J. Holmes, and S. R. Forrest, Prospects for electrically pumped organic lasers, Phys. Rev. B **66**, 035321 (2002).

[13] N. C. Giebink and S. R. Forrest, Temporal response of optically pumped organic semiconductor lasers and its implication for reaching threshold under electrical excitation, Phys. Rev. B **79**, 073302 (2009).

[14] N. Tessler, D. J. Pinner, V. Cleave, D. S. Thomas, G. Yahioglu, P. Le Barny, and R. H. Friend, Pulsed excitation of low-mobility light-emitting diodes: Implication for organic lasers, Appl. Phys. Lett. **74**, 2764 (1999).

[15] V. G. Kozlov, G. Parthasarathy, P. E. Burrows, V. B. Khalfin, J. Wang, S. Y. Chou, and S. R. Forrest, Structures for organic diode lasers and optical properties of organic semiconductors under intense optical and electrical excitations, IEEE J. Quantum Electron. **36**, 18 (2000).

[16] The lowest theoretical limit of the electrically driven threshold in organic semiconductor material is about 80 A cm^{-2} [15]. It was estimated from the value of the optically pumped threshold under assumption of maximum recombination rate and neglecting the current-induced losses and metal contact [17], since the lowest reported threshold under optical pumping is of the order of 100 Wcm^{-2}, reached in conjugated polymers [18].

[17] M. D. McGehee and A. J. Heeger, Semiconducting (conjugated) polymers as materials for solid-state lasers, Adv. Mater. **12**, 1655 (2000).

[18] R. Gupta, M. Stevenson, and A. J. Heeger, Low threshold distributed feedback lasers fabricated from blends of conjugated polymers: Reduced losses through Förster transfer, J. Appl. Phys. **92**, 4874 (2002).

[19] T. Voss, D. Scheel, and W. Schade, A microchip-laser-pumped DFB-polymer-dye laser, Appl. Phys. B **73**, 105 (2001).

[20] T. Riedl, T. Rabe, H.-H. Johannes, W. Kowalsky, J. Wang, T. Weimann, P. Hinze, B. Nehls, T. Farrell, and U. Scherf, Tunable organic thin-film laser pumped by an inorganic violet diode laser, Appl. Phys. Lett. **88**, 241116 (2006).

[21] A. E. Vasdekis, G. Tsiminis, J.-C. Ribierre, L. O' Faolain, T. F. Krauss, G. A. Turnbull, and I. D. W. Samuel, Diode pumped distributed Bragg reflector lasers based on a dye-to-polymer energy transfer blend, Opt. Express **14**, 9211 (2006).

[22] Y. Yang, G. A. Turnbull, and I. D. W. Samuel, Hybrid optoelectronics: A polymer laser pumped by a nitride light-emitting diode, Appl. Phys. Lett. **92**, 163306 (2008).

[23] M. A. Noginov, G. Zhu, A. M. Belgrave, R. Bakker, V. M. Shalaev, E. E. Narimanov, S. Stout, E. Herz, T. Suteewong, and U. Wiesner, Demonstration of a spaser-based nanolaser, Nature (London) **460**, 1110 (2009).

[24] M. Gather, K. Meerholz, N. Danz, and K. Leosson, Net optical gain in a plasmonic waveguide embedded in a fluorescent polymer, Nat. Photon. **4**, 457 (2010).

[25] X. Meng, J. Liu, A. V. Kildishev, and V. M. Shalaev, Highly directional spaser array for the red wavelength region, Laser Photon. Rev. **8**, 896 (2014).

[26] S. Y. Lam and M. J. Damzen, Characterisation of solid-state dyes and their use as tunable laser amplifiers, Appl. Phys. B **77**, 577 (2003).

[27] V. Bulovic, V. G. Kozlov, V. B. Khalfin, and S. R. Forrest, Transform-limited, narrow-linewidth lasing action in organic semiconductor microcavities, Science **279**, 553 (1998).

[28] W. Lu, B. Zhong, and D. Ma, Amplified spontaneous emission and gain from optically pumped films of dye-doped polymers, Appl. Opt. **43**, 5074 (2004).

[29] A. Costela, O. Garcia, L. Cerdan, I. Garcia-Moreno, and R. Sastre, Amplified spontaneous emission and optical gain measurements from pyrromethene 567—doped polymer waveguides and quasi-waveguides, Opt. Express **16**, 7023 (2008).

[30] M. Lebental, E. Bogomolny, and J. Zyss, Organic microlasers: A new avenue onto wave chaos physics, in *Practical Applications of Micro-resonators in Optics and Photonics*, edited by A. Matsko (CRC, Boca Raton, 2009), pp. 317–354.

[31] M. Lebental, N. Djellali, C. Arnaud, J.-S. Lauret, J. Zyss, R. Dubertrand, C. Schmit, and E. Bogomolny, Inferring periodic orbits from spectra of simply shaped microlasers, Phys. Rev. A **76**, 023830 (2007).

[32] J. R. Lakowicz, *Principles of Fluorescence Spectroscopy*, 3rd ed. (Springer, New York, 2006).

[33] B. Valeur, *Molecular Fluorescence: Principles and Applications* (Wiley-VCH, New York, 2001).

[34] Gain values in dB [g(dB)] represent an overall sample amplification and may be recalculated to g(cm^{-1}) using the expression $10^{g(dB)/10}/l$(cm), where l (cm) is the sample length in cm.

[35] L. Dal Negro, P. Bettotti, M. Cazzanelli, D. Pacifici, and L. Pavesi, Applicability conditions and experimental analysis of the variable stripe length method for gain measurements, Opt. Commun. **229**, 337 (2004).

[36] L. A. Coldren and S. W. Corzine, *Diode Lasers and Photonic Integrated Circuits*, Wiley Series in Microwave and Optical Engineering (Wiley, New York, 1995).

[37] O. G. Peterson, J. P. Webb, W. C. McColgin, and J. H. Eberly, Stimulated emission from flashlamp-excited organic dyes in polymethyl Methacrylate, J. Appl. Phys. **42**, 1917 (1971).

[38] A. Tagaya, Y. Koike, E. Nihei, S. Teramoto, K. Fujil, T. Yamamoto, and K. Sasaki, Basic performance of an organic dye-doped polymer optical fiber amplifier, Appl. Opt. **34**, 988 (1995).

[39] H. Rabbani-Haghighi, S. Forget, S. Chénais, A. Siove, M.-C. Castex, and E. Ishow, Gain measurement and low-threshold laser operation in non-doped thin films made of a small-molecule organic red-emitter, Appl. Phys. Lett. **95**, 033305 (2009).

[40] J. Valenta, I. Pelant, and J. Linnros, Waveguiding effects in the measurement of optical gain in a layer of Si nanocrystals, Appl. Phys. Lett. **81**, 1396 (2002).

[41] E. Smotrova, V. Byelobrov, T. Benson, J. Ctyroký, R. Sauleau, and A. Nosich, Optical theorem helps understand thresholds of lasing in microcavities with active regions, IEEE J. Quantum Electron. **47**, 20 (2011).

[42] S. W. Corzine, R. S. Geels, J. W. Scott, R-H. Yan, and L. A. Coldren, Design of Fabry-Perot surface-emitting lasers with a periodic gain structure, IEEE J. Quantum Electron. **25**, 1513 (1989).

[43] I. Gozhyk, G. Clavier, R. Méallet-Renault, M. Dvorko, R. Pansu, J.-F. Audibert, A. Brosseau, C. Lafargue, V. Tsvirkun, S. Lozenko, S. Forget, S. Chénais, C. Ulysse, J. Zyss, and M. Lebental, Polarization properties of solid-state organic lasers, Phys. Rev. A **86**, 043817 (2012).

[44] There is no significant difference whatever is plotted— maximum of a spectrum or sum over all the pixels—and how the threshold intensity is determined from the plot.

[45] S. Lozenko, N. Djellali, I. Gozhyk, C. Delezoide, J. Lautru, C. Ulysse, J. Zyss, and M. Lebental, Enhancing performance of polymer-based microlasers by a pedestal geometry, J. Appl. Phys. **111**, 103116 (2012).

[46] D. Yokoyama, Molecular orientation in small-molecule organic light-emitting diodes, J. Mater. Chem. **21**, 19187 (2011).

[47] D. Yokoyama, A. Sakaguchi, M. Suzuki, and C. Adachi, Horizontal orientation of linear-shaped organic molecules having bulky substituents in neat and doped vacuum-deposited amorphous films, Org. Electron. **10**, 127 (2009).

[48] S. Bidault, S. Brasselet, and J. Zyss, Coherent control of the optical nonlinear and luminescence anisotropies in molecular thin films by multiphoton excitations, Opt. Lett. **29**, 1242 (2004).

[49] O. I. Yaroshenko, Theory of pulsed dye lasers with account of optical anisotropy and rotational diffusion, J. Opt. A **5**, 328 (2003).

[50] K. C. Reyzer and L. W. Casperson, Polarization characteristics of dye-laser amplifiers I. Unidirectional molecular distributions, J. Appl. Phys. **51**, 6075 (1980).

[51] K. C. Reyzer and L. W. Casperson, Polarization characteristics of dye-laser amplifiers II. Isotropic molecular distributions, J. Appl. Phys. **51**, 6083 (1980).

[52] P. Liang, Q. Chen, S. Zhang, and J. Lei, Polarization and power characteristics of pulsed dye lasers with transverse pumping, Appl. Phys. B **55**, 494 (1992).

[53] I. Gozhyk, S. Forget, S. Chénais, C. Ulysse, A. Brosseau, R. Méallet-Renault, G. Clavier, R. Pansu, J. Zyss, and M. Lebental, Towards polarization controlled organic micro-lasers, Proc. SPIE **8258**, 82580K (2012).

[54] D. Wright, E. Brasselet, J. Zyss, G. Langer, and W. Kern, Dye-doped organic distributed-feedback lasers with index and surface gratings: Role of pump polarization and molecular orientation, J. Opt. Soc. Am. B **21**, 944 (2004).

[55] P. Selenyi, Wide angle interferences and the nature of elementary light sources, Phys. Rev. **56**, 477 (1939).

[56] There is an error in Eq. (6) of [53]. It should read $\cos 2\varphi \cos 2\alpha$ instead of $\cos(2\varphi + 2\alpha)$.

[57] L. W. Casperson, W. J. Sandle, A. C. Wilson, D. M. Warrington, and R. J. Ballagh, Pump polarization effects in cw dye lasers, J. Appl. Phys. **69**, 8005 (1991).

[58] V. Le Floc'h, S. Brasselet, J.-F. Roch, and J. Zyss, Monitoring of orientation in molecular ensemblesby polarization sensitive nonlinear microscopy, J. Phys. Chem. B **107**, 12403 (2003).

[59] E. Bogomolny, N. Djellali, R. Dubertrand, I. Gozhyk, M. Lebental, C. Schmit, C. Ulysse, and J. Zyss, Trace formula for dielectric cavities II: Regular, pseudo-integrable, and chaotic examples, Phys. Rev. E **83**, 036208 (2011).

[60] M. M. Mazumder, G. Chen, P. J. Kindlmann, R. K. Chang, and J. B. Gillespie, Temperature-dependent wavelength shifts of dye lasing in microdroplets with a thermochromic additive, Opt. Lett. **20**, 1668 (1995).

[61] H. Taniguchi and H. Tomisawa, Wavelength shifts of a suspended-single-droplet dye laser by successive laser pumping, Opt. Lett. **19**, 1852 (1994).

[62] V. Baev, T. Latz, and P. Toschek, Laser intracavity absorption spectroscopy, Appl. Phys. B **69**, 171 (1999).

[63] H. Rabbani-Haghighi, S. Forget, A. Siove, and S. Chénais, Analytical study of vertical external-cavity surface-emitting organic lasers, Eur. Phys. J. Appl. Phys. **56**, 34108 (2011).

[64] B. Crenshaw, J. Kunzelman, C. Sing, C. Ander, and C. Weder, Threshold temperature sensors with tunable properties, Macromol. Chem. Phys. **208**, 572 (2007).

[65] J. A. E. Wasey, A. Safonov, I. D. W. Samuel, and W. L. Barnes, Efficiency of radiative emission from thin films of a light-emitting conjugated polymer, Phys. Rev. B **64**, 205201 (2001).

[66] J. A. Spitz, R. Yasukuni, N. Sandeau, M. Takano, J. J. Vachon, R. Meallet-Renault, and R. B. Pansu, Scanning-less wide-field single-photon counting device for fluorescence intensity, lifetime and time-resolved anisotropy imaging microscopy, J. Microsc. **229**, 104 (2008).

[67] M. Pope and C. Swenberg, *Electronic Processes in Organic Crystals and Polymers* (Oxford University Press, New York, 1999).

[68] S. L. Bondarev, V. N. Knyukshto, V. I. Stepuro, A. P. Stupak, and A. A. Turban, Fluorescence and electronic structure of the laser dye DCM in solutions and in polymethylmethacrylate, J. Appl. Spectrosc. **71**, 194 (2004).